

Distribution and expression of gas seeps in a gas hydrate province of the northeastern Sakhalin continental slope, Sea of Okhotsk

Young Keun Jin ^{a,*}, Young-Gyun Kim ^a, Boris Baranov ^b, Hitoshi Shoji ^c, Anatoly Obzhairov ^d

^a Korea Polar Research Institute, Songdo-dong, Yeosu-gu, Incheon 406-840, South Korea

^b P.P. Shirshov Institute of Oceanology, RAS, 36 Nakhimovkii Prospect, Moscow 117218, Russia

^c New Energy Resources Research Center, Kitami Institute of Technology, 165 Koen-cho, Kitami 090-8507, Japan

^d V.I. Il'ichev Pacific Oceanological Institute, FEB RAS, 43 Baltiyskaya Street, Vladivostok 690041, Russia

ARTICLE INFO

Article history:

Received 13 March 2010

Received in revised form

21 January 2011

Accepted 15 March 2011

Available online 21 March 2011

Keywords:

Gas seep

Gas hydrate

Active seepage

Sakhalin continental slope

Okhotsk Sea

ABSTRACT

Multidisciplinary surveys were conducted to investigate gas seepage and gas hydrate accumulation on the northeastern Sakhalin continental slope (NESS), Sea of Okhotsk, during joint Korean–Russian–Japanese expeditions conducted from 2003 to 2007 (CHAOS and SSGH projects). One hundred sixty-one gas seeps were detected in a 2000 km² area of the NESS (between 53°45'N and 54°45'N). Active gas seeps in a gas hydrate province on the NESS were evident from features in the water column, on the seafloor, and in the subsurface: well-defined hydroacoustic anomalies (gas flares), side-scan sonar structures with high backscatter intensity (seepage structures), bathymetric structures (pockmarks and mounds), gas- and gas-hydrate-related seismic features (bottom-simulating reflectors, gas chimneys, high-amplitude reflectors, and acoustic blanking), high methane concentrations in seawater, and gas hydrates in sediment near the seafloor. These expressions were generally spatially related; a gas flare would be associated with a seepage structure (mound), below which a gas chimney was present. The spatial distribution of gas seeps on the NESS is controlled by four types of geological structures: faults, the shelf break, seafloor canyons, and submarine slides. Gas chimneys that produced enhanced reflection on high-resolution seismic profiles are interpreted as active pathways for upward gas migration to the seafloor. The chimneys and gas flares are good indicators of active seepage.

© 2011 Elsevier Ltd. All rights reserved.

1. Introduction

Gas seeps are widespread in the marine sediment of modern continental margins (Judd and Hovland, 2007). The release of methane through gas seeps has attracted growing attention from scientific communities because of their potential impact on the geosphere, biosphere, hydrosphere, and atmosphere (Judd, 2003). These seeps can be part of a gas hydrate system (Kvenvolden, 1993).

Particularly large methane releases from gas hydrate systems may explain certain episodes in the geological record that were characterized by sudden global warming and massive increases in atmospheric carbon, such as the Paleocene–Eocene thermal maximum (Dickens et al., 1995; Katz et al., 1999) and the terminations of Quaternary glaciations (Paull et al., 1991; Kennett et al., 2000). Modern gas releases from marine gas hydrate systems have been observed at the Cascadia Margin (Heeschen et al., 2003),

in the Gulf of Mexico (MacDonald et al., 2002), in the Black Sea (Greiner et al., 2006), and in many other places throughout the world (Sauter et al., 2006; Naudts et al., 2010). Although these releases are modest in comparison with the catastrophic releases that would be needed to explain sudden global warmings of the geologic past, they can provide important information about how gas can migrate through the gas hydrate system and into the ocean and atmosphere, and how gas seeps contribute to atmospheric methane concentrations.

Active gas seeps are widespread in the Sea of Okhotsk. Gas hydrate and gas seeps are known from offshore Paramushir Island and the northeastern Sakhalin slope (NESS) (Zonenshayn et al., 1987; Ginsburg et al., 1993; Soloviev et al., 1994; Soloviev and Ginsburg, 1994, 1997; Gaedicke et al., 1997). On the NESS, gas seeps were recognized by gas “flares” (gas bubble streams in the water column) on echograms and high methane anomalies in the water column (Obzhairov, 1992; Ginsburg et al., 1993; Soloviev and Ginsburg, 1994, 1997). More than 100 gas flares were detected and gas hydrates were recovered during the expeditions of the German–Russian KOMEX Project (Biebow and Hutten, 1999;

* Corresponding author. Tel.: +82 32 260 6212.

E-mail address: ykjin@kopri.re.kr (Y.K. Jin).

Biebow et al., 2003; Matveeva et al., 2003). These results led to further detailed investigation of a gas hydrate province on the NESS. Two international projects, CHAOS (Carbon Hydrate Accumulations in the Okhotsk Sea) and SSGH (Sakhalin Slope Gas Hydrates), have been carried out since 2003 to investigate gas seepage and gas hydrate accumulation in the NESS.

This paper describes hundreds of gas seeps and a range of associated geological features that were discovered on the north-eastern Sakhalin continental slope during the CHAOS (2003, 2005, 2006) and SSGH (2007) projects. The spatial distribution of gas seeps and their controlling factors, evidence of active gas seepage,

and subsurface features beneath active gas seeps are discussed and interpreted.

2. Geological settings

The Sea of Okhotsk, one of the marginal seas that rim the Pacific, is located predominantly over the Okhotsk Plate, which is bordered across transform boundaries by the Eurasian, North American, and Amur plates, and across a convergent boundary by the Pacific Plate (Fig. 1). The Sakhalin Shear Zone (SSZ), a transform boundary between the Okhotsk and Amur plates, extends longitudinally over

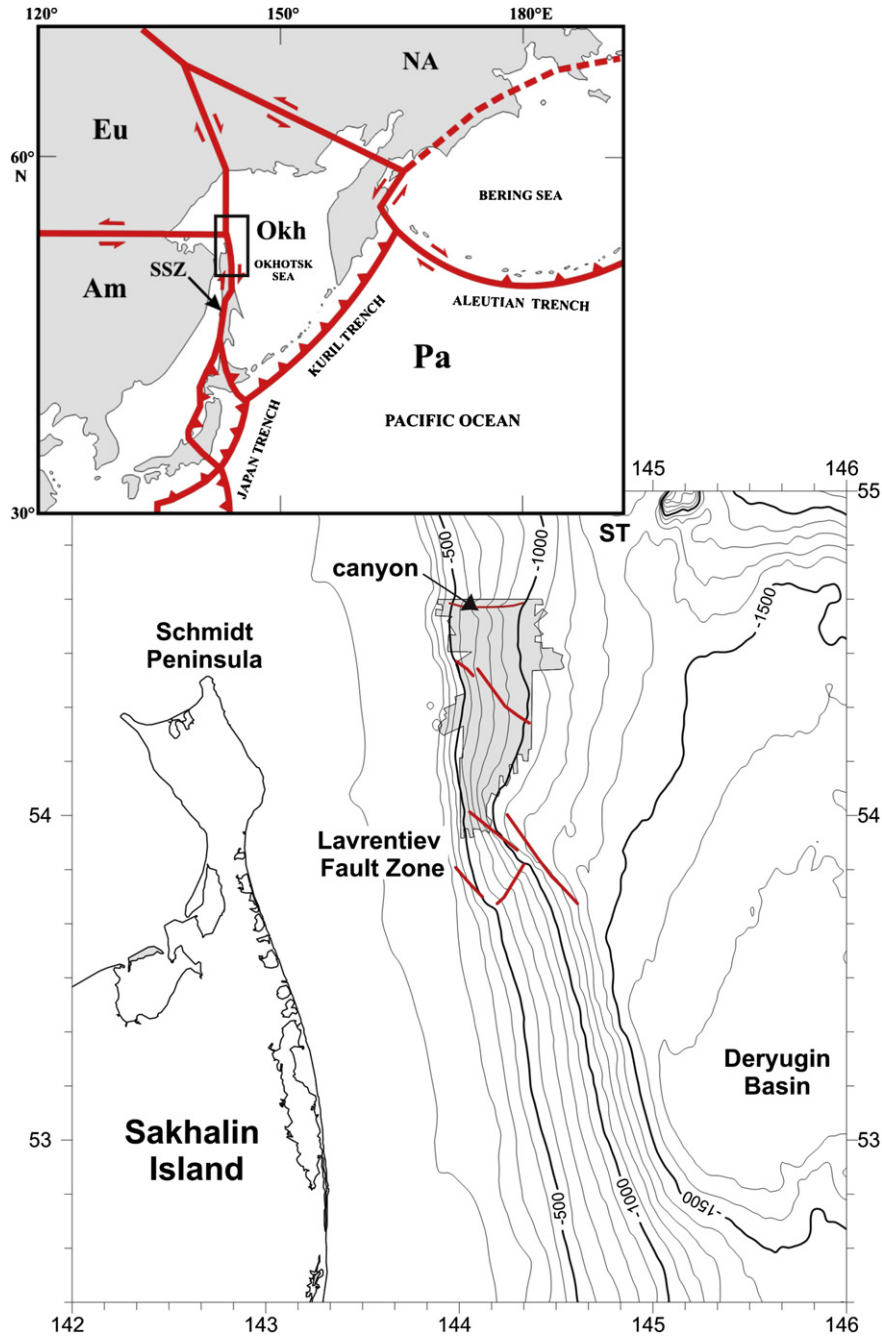


Figure 1. Tectonic and Bathymetric map of the northeastern Sakhalin slope. Box in the tectonic map indicates the study area. In the bathymetric map, gray area indicates the side-scan sonar mapping area shown in Fig. 2, and red lines indicate faults and a canyon that appear as seafloor features. Contour interval is 100 m. Eu = Eurasian Plate, Na = North American Plate, Am = Amur Plate, Okh = Okhotsk Plate, Pa = Pacific Plate, SSZ = Sakhalin Shear Zone, ST = Stareztkiy Trough. (For interpretation of the references to colour in this figure legend, the reader is referred to the web version of this article.)

a distance of 2000 km, crossing Sakhalin Island and the western part of Hokkaido Island. The SSZ consists of north-trending dextral strike-slip faults associated conjugate thrusts and reverse faults in Sakhalin Island (Rozhdestvenskiy, 1986; Fournier et al., 1994). Most of this fault system is not exposed on the surface due to a thick sediment cover, but its location is clearly traced by intensive seismicity (Tikhonov and Kim, 2010).

The eastern slope of Sakhalin Island contains a very thick sedimentary succession that is approximately 9–14 km thick (Kharakhinov, 1998) and overlies the area of most rapid subsidence. The thickness of the sedimentary package and underlying acoustic basement are poorly defined on seismic profiles due to saturation of sediments by gas (Worrall et al., 1996). The sedimentary succession is thought to represent a delta system that predated the present-day Amur River delta (Kharakhinov, 1998). The Schmidt Rise separates the NESS from the northeastern Sakhalin shelf, of

which the stratigraphy is well known as a result of exploration drilling and correlation with outcrops on land (Sergeev, 2004).

The sedimentary succession of this area is known to have a favorable hydrological regime for methane gas accumulation: high primary productivity in the water column and high sedimentation rates produced a high organic carbon content in the sediment (>1.5%; Gorbarenko et al., 1990; Astakhov et al., 2000). The vertical temperature profile of the Sea of Okhotsk is also favorable for methane gas hydrate, exhibiting a marked temperature decrease from the sea surface to 100 m of water depth, where the thermal minimum of $-1\text{ }^{\circ}\text{C}$ is reached, and then a steady increase to $2\text{ }^{\circ}\text{C}$ at 600–800 m depth (Matveeva et al., 2005; Mazurenko et al., 2006). The top of the gas hydrate stability zone in the water column is expected to be very shallow, around 300 m water depth.

Wong et al. (2003) described Quaternary sedimentation in the northwestern Sea of Okhotsk using high-resolution seismic data.

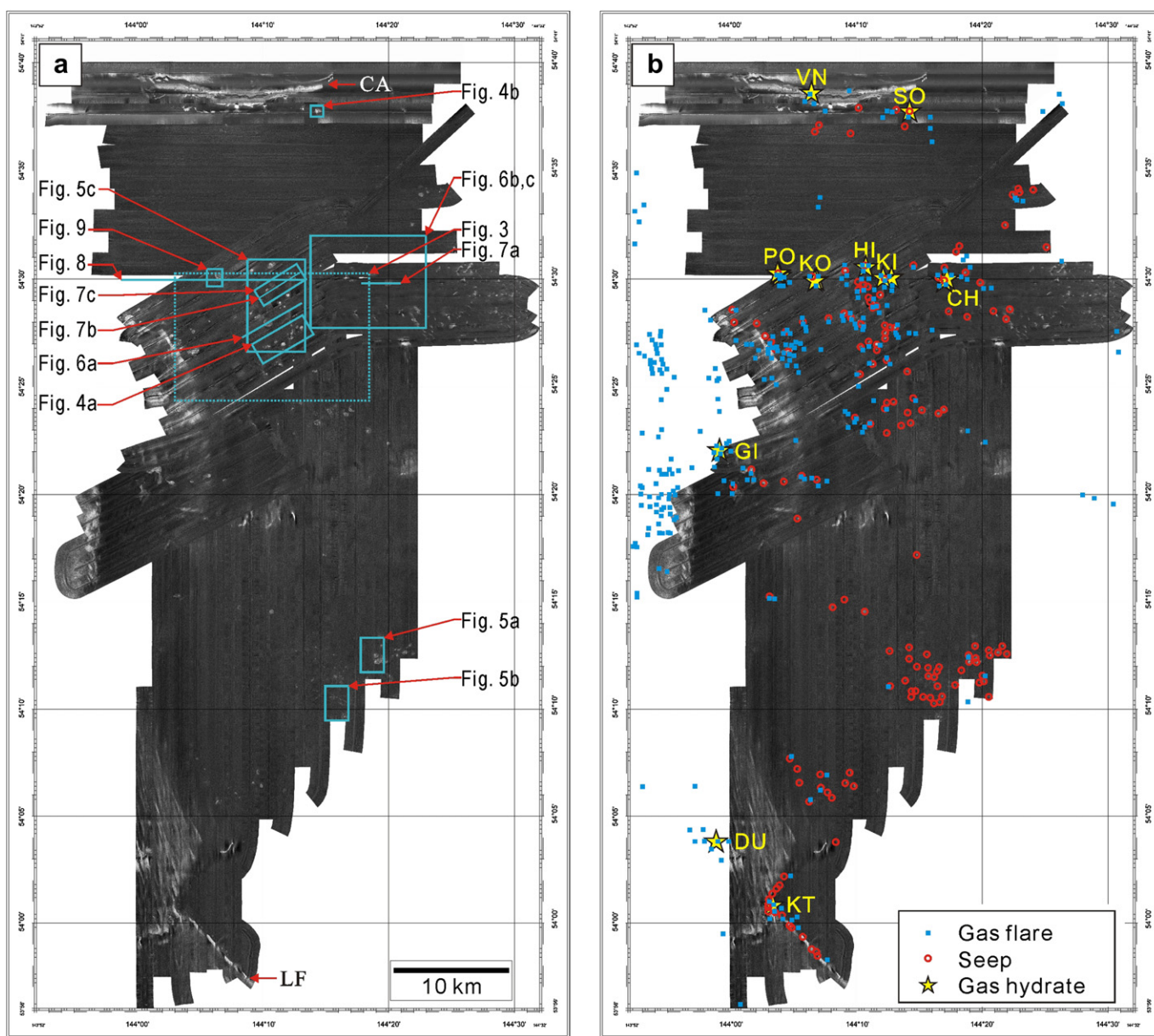


Figure 2. Side-scan sonar mosaic with (a) locations of figures (rectangles and lines), CA = canyon; LF = Lavrentyev fault and (b) locations of gas flares (blue squares), seeps (red circles), and sampling sites of gas hydrates (yellow stars): CH = CHAOS, DU = Dungeon, GI = Gisella, HI = Hieroglyph, KI = Kitami, KO = KOPRI, KT = KIT, VN = VNIIOkeangeologia, SO = Soloviev, PO = POI structures. (For interpretation of the references to colour in this figure legend, the reader is referred to the web version of this article.)

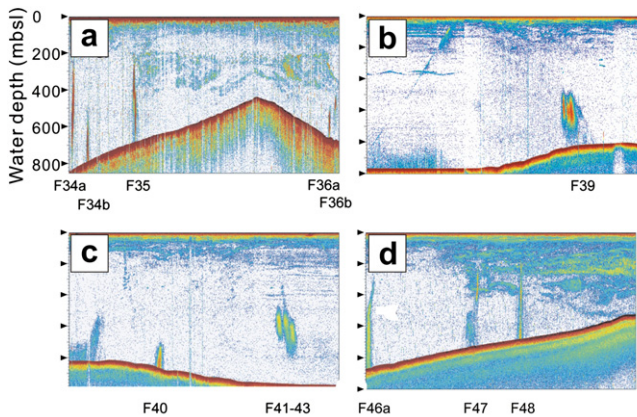


Figure 3. Images of gas flares documented by hydroacoustic survey. Various shapes of gas flares were detected: (a) linear, (b) and (c) floating, and (d) deformed. Flares commonly extended from the seafloor to a shallow depth of 200 m. Triangles denote

According to their work, sedimentation in this area is characterized mainly by bottom current-controlled processes and mass wasting. Bottom current-controlled processes lead to widespread deposition of contourite drifts and sediment waves on the North Okhotsk continental margin and the northernmost Sakhalin slope, as well as to erosion and sediment reworking on the northern Sakhalin shelf. Mass-wasting deposits with massive reflector-poor facies are widespread in the western Deryugin Basin. Repeated mass wasting that has probably changed the original convex cross-section of the slope in the study area to a concave form, excavating large volumes of sediments which are deposited as slumps and debris flows in the western Deryugin Basin. These mass wasting events are thought to have been triggered probably by shallow earthquakes or by gas hydrate instability during sea-level lowstands.

3. Materials and methods

The CHAOS (2003, 2005, 2006) and SSGH (2007) expeditions were conducted on the NESS between 53°45'N and 54°45'N using the Russian research vessel *Academician Lavrentyev* (Fig. 1). Multidisciplinary data sets were obtained during these expeditions: hydroacoustic profiling using single-beam echosounders, seafloor imaging using side-scan sonar (SSS), seismic reflection profiling using a sub-bottom profiler and sparker-source seismic system, CTD profiling, water-sampling using a rosette sampler, and near-bottom gas hydrate sampling using a gravity hydro-corer.

Gas bubbles in the water column have high impedance contrast relative to water and appear on echograms as hydroacoustic anomalies with flared shapes (gas “flares”). The hydroacoustic systems ‘ELAC’ and/or ‘Sargan-EM’ were used simultaneously with

frequencies of 12, 20, and 135 kHz to detect gas flares (Salomatin et al., 2008).

Deep-tow side-scan sonar surveys were conducted using the ‘SONIC-3’ system with a frequency of 30 kHz in a medium-range mode and a swath range of 800–3200 m. Width range is 500–2000 m, and the best resolution is 2.0 m. The ‘SONIC-3M’ system is also equipped with a sub-bottom profiler with a frequency of 8 kHz (maximum resolution = 0.3 m). The sonar “fish” was towed at 90–120 m above the seafloor and ship speed was 2–4 knots.

High-resolution seismic data were obtained using the ‘SONIC-4’ sparker system made in Russia. The system used a sparker with a frequency range of 200–1200 Hz and an energy of 500–2000 J as a source, and a single-channel streamer as a receiver. The system provides a resolution of 2–5 m for sediment layer thickness and a bottom penetration of 50–300 m.

To measure methane concentrations in the water column, water samples were taken using a rosette water sampler combined with CTD. Gas extracted from water and preserved from contact with the atmosphere was analyzed on the ship using an SRI 8160C chromatograph. Sediment cores to sample gas hydrates were retrieved using a 5.5-m-long ‘GSP-2’ gravity hydro-corer.

4. Evidence of active gas seeps

4.1. Gas flares in the water column

More than 300 gas flares were detected in the NESS (blue squares in Fig. 2b). Their locations concur with known seep locations, indicating that the gas was emitted from active seeps. Figure 3 shows typical examples of detected gas flares. Most of the gas flares rise vertically from the seafloor to some elevation in the water column and have profile widths of up to 100 m. Their heights range from several tens to several hundred meters; for example, F34a rises 600 m above the seafloor (Fig. 3a). Flares F39 and F41–43 were “floating” rather than rooted to the seafloor (Fig. 3b and c), a phenomenon that can be explained by: 1) a gas flare rising obliquely from a seeping site that is located out of the plane of the hydroacoustic survey track, or 2) gas emission that is intermittent or varies with time. Flares F40 and F46a are associated with the same seep (‘Kitami Structure’, see Fig. 2b for location) with a time difference of approximately 12 h, and rose to 160 and 700 m, respectively (Fig. 3c and d). Such variation of flare heights may be indicative of temporally variable gas flux, but may be caused by slight difference in vessel location and/or changing near-bottom current.

Some gas flares (F35 and F47–48) persist up to water depths of 150–250 m (Fig. 3a and d), which is much shallower than the ~300 m depth of the expected upper boundary of the gas hydrate stability zone (GHSZ), as expected for a seawater temperature of

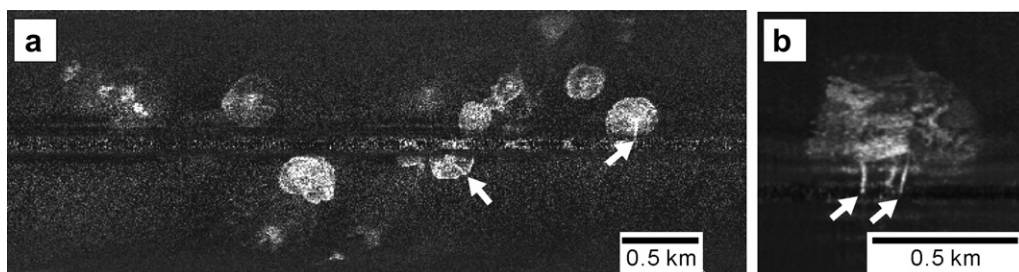


Figure 4. Gas flares documented by side-scan sonar survey. (a) Obvious flares (arrows) emitted from elevated backscattering structures and (b) two flares emitted from a single high backscatter area inside the Soloviev structure. See Fig. 2 for location.

2 °C (Dickens and Quinby-Hunt, 1994). Rising gas bubbles could survive within the GHSZ and reach the upper boundary of the GHSZ due to the formation of gas-hydrate skin preventing rapid dissociation in the water column (Heeschen et al., 2003; Greinert et al., 2006). The persistence of gas flares close to the sea surface in the study area may be attributed to cold temperature of the shallow water column (−1 °C to 1 °C in 100 m–300 m water depth).

Gas flares are occasionally well imaged on side-scan sonar mosaics as bright strings (indicated by arrows in Fig. 4). In Figure 4b gas emanates from the sides of the central high backscatter anomaly. The right flare in Figure 4a and both flares in Figure 4b reached the center beam of the sonar, which implies that the flares rose at least as far as the sonar fish, which was towed about 100 m above the seafloor.

4.2. Seepage structures on the seafloor

Side-scan sonar (SSS) surveys were undertaken during CHAOS and SSGH projects expeditions (2003, 2006, and 2007). Survey areas covered the northeast continental slope between 53°57.5'N and 54°40'N at water depths of 300–1100 m (Figs. 1 and 2). New SSS data reveal that seafloor structures with high backscatter intensity, which are interpreted as the seepage structures, are common on the slope.

Based on the SSS mosaic (Fig. 2a), 161 identified seepage structures (squares in Fig. 2b) were classified according to shape and backscatter intensity. Chemical and isotope analyses of interstitial and hydrate waters/gases from major hydrate-rich venting structures (CHAOS, Gisella, Hieroglyph, Kitami, KOPRI, POI, and VNIIOkeangeologia, see Fig. 2b for their locations) were presented and interpreted in relation

to the hydrate-forming fluid (Mazurenko et al., 2009; Hachikubo et al., 2010). The seepage structures have circular, linear, and angular outlines. The circular seeps are most common and have a diameter ranging from 100 to 800 m (Fig. 5a and c). Linear- or angular-shaped seeps (Fig. 5b) are present only in the southern part of the study area. The linear-shaped seep shown in Figure 5b is about 50 m wide and 2 km long and trends northwest, with a west-trending branch near its middle. This seep's length and bifurcation suggest that it may be associated with an underlying fault or fissure.

4.3. Bathymetric expression

Positive and negative topographic features on the seafloor are common in echosounder and bathymetric surveys and indicate a physical interaction between methane flux and sediment (e.g., Fig. 6; Hovland and Judd, 1988). Positive features (mounds) are 5–8 m high and several hundred meters wide. Gas flares commonly rise from the mounds (F36a and b in Fig. 3a, and two flares in Fig. 6a). The mounds probably form through the upward migration of overpressured fluid from below. Negative features (pockmarks) are up to several hundred meters in diameter and several tens of meters deep (Fig. 6b).

Comparison of these bathymetric features with backscatter structures (Fig. 6b and c) shows that the three mounds correlate with high-backscatter structures (denoted as 4.4, 4.8 and 4.13). No consistent correlation exists for the pockmarks (4.5, 4.9, 4.10, and 4.12 in Fig. 8). High backscatter intensity is associated with the center or margin of some pockmarks, but others do not appear on the SSS mosaics at all.

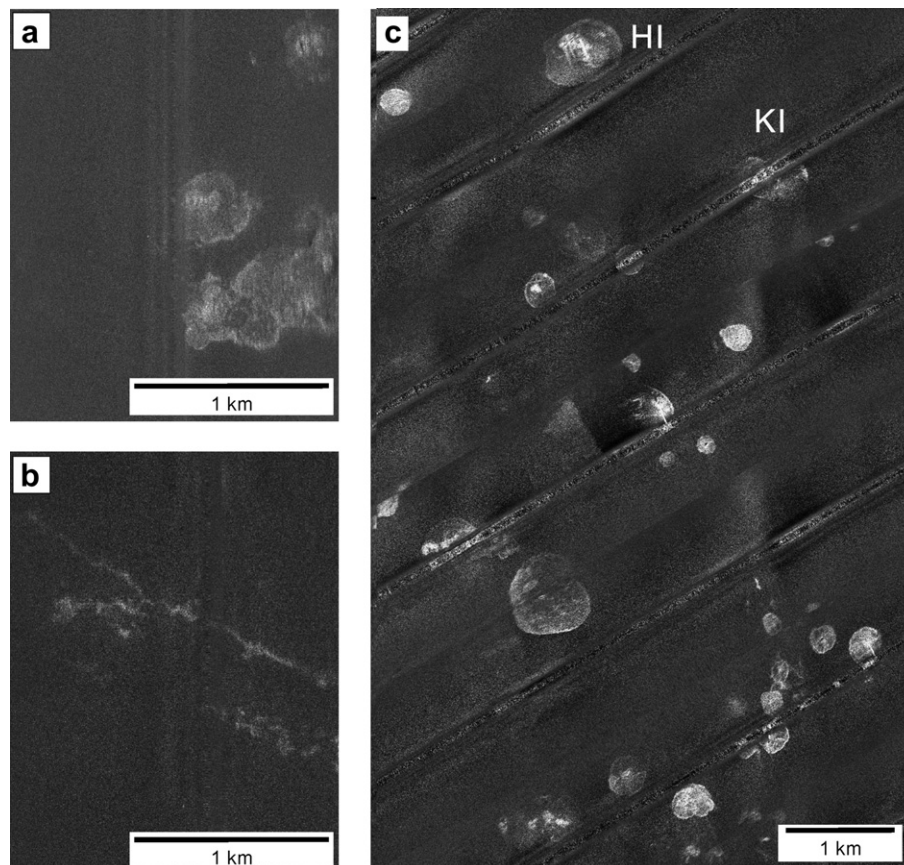


Figure 5. High-backscatter areas documented in side-scan sonar survey. (a) Irregular, (b) linear, and (c) circular high backscatter areas. Irregular shapes represent coalesced circular zones. Linear high backscatter area is over 1 km long. Diameter of circular areas reaches several hundred meters. HI=Hieroglyph, KI = Kitami structures. See Fig. 2 for location.

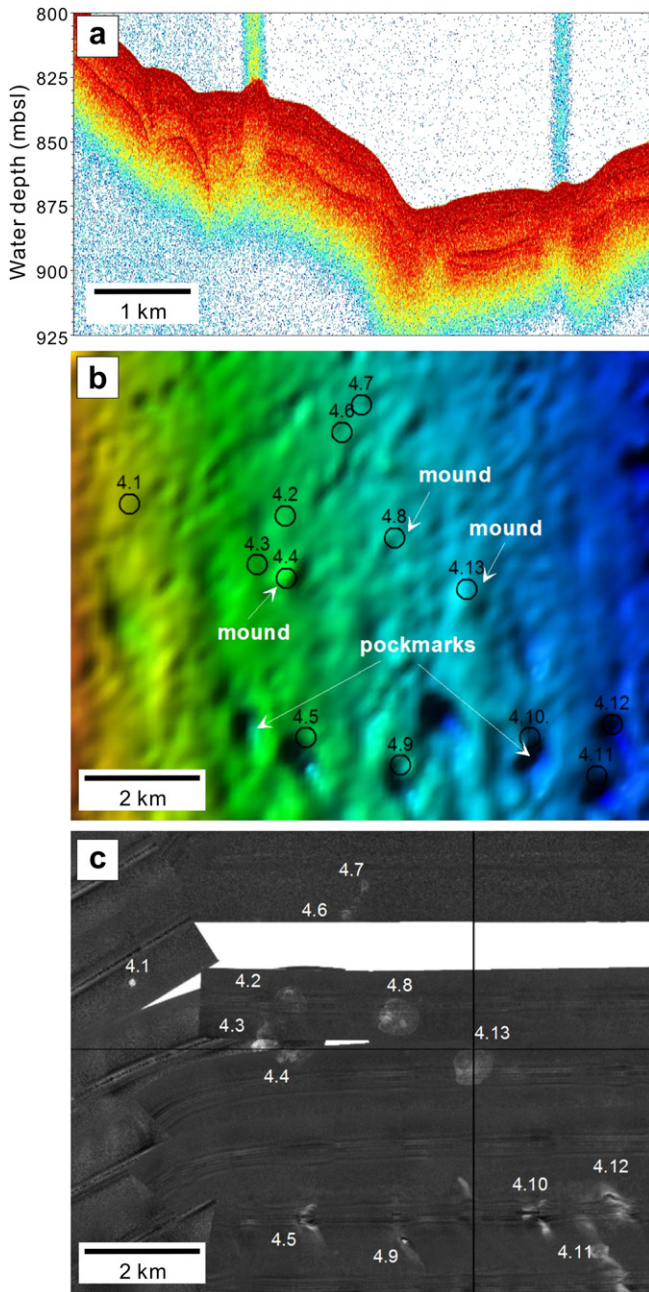


Figure 6. Pockmarks and mounds illustrated by (a) 12-kHz hydroacoustic profile, (b) swath bathymetry, and (c) side-scan sonar image. Gas flares emitted from mounds are conspicuous in (a). The high backscatter area in (c) correlates with mound and pockmark distribution (b), although the strongest backscattering is associated only with mounds. Loci which are denoted as 4.2, 4.3, and 4.4 correspond the CHAOS structure.

4.4. Subsurface features

Geophysical surveys identified various subsurface features, including acoustic blanking, bottom-simulating reflectors, high-amplitude reflectors, and seismic chimneys.

4.4.1. Acoustic blanking

Hydroacoustic profiles obtained using a 12-kHz echosounder show subsurface reflectors up to approximately 30 m below the seafloor (mbsf) as well as gas flares in the water column. For example, Figure 7a shows a well-stratified, strong reflector at about

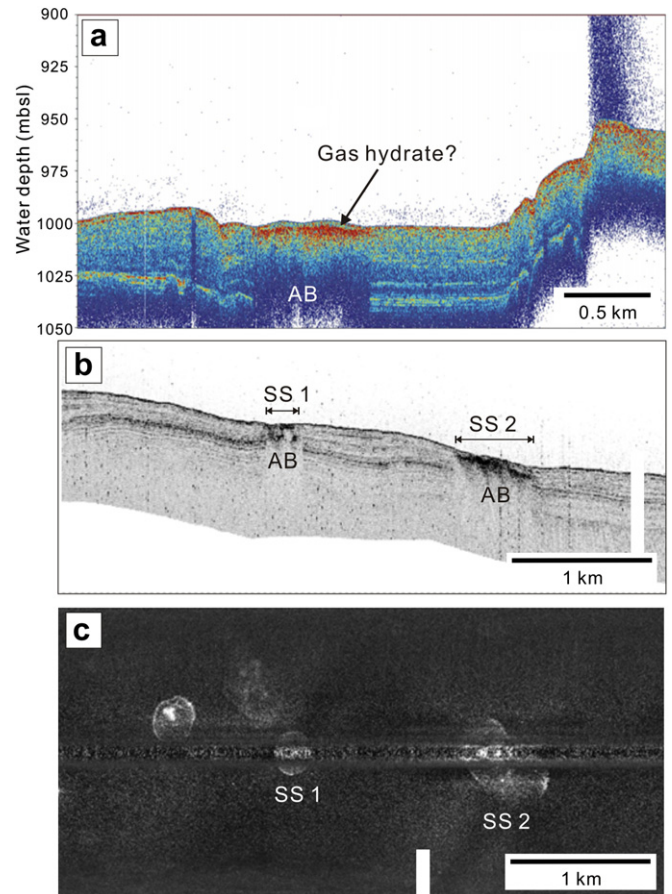


Figure 7. Zones of acoustic blanking documented in (a) hydroacoustic profile and (b) sub-bottom profile. Acoustic blanking (AB) may result from sub-bottom gas-bearing sediment or near-bottom gas hydrate layers that inhibit signal penetration. Seeps SS1 and SS2 exhibit acoustic blanking on the sub-bottom profile (b) and high backscatter intensity in a side-scan sonar image (c). SS2 corresponds to the Kitami structure. See Fig. 2 for location.

25 mbsf that is interrupted by acoustic blanking (a zone devoid of reflection) below a seepage structure. The top of the acoustic blanking, at ~5 mbsf, is a very strong reflector. The width of the acoustic blanking is identical to that of this strong reflector. Although this kind of acoustic blanking is common on high-resolution shallow seismic profiles in areas where gas is present (Judd and Hovland, 2007), its occurrence in a deep-sea area that is in the GHSZ is unique. There are two possible explanations for this blanking: 1) attenuation of seismic energy owing to the presence of free gas, or 2) poor seismic energy penetration owing to strong reflection from a near-surface reflector that overlies the blanking. In the latter case, the reflector could be a layer of gas hydrate or methane-derived authigenic carbonate. Near-surface gas hydrates were sampled at several major seeps using a 5.5 m-long gravity corer during the CHAOS expeditions (Mazurenko et al., 2009).

Acoustic blanking also appears on sub-bottom profiles that were obtained at the same time as side-scan sonar images (Fig. 7b). The extent of the acoustic blanking zones is in good agreement with the dimension of their overlying seepage structures on the SSS mosaic (Fig. 7b and c).

4.4.2. Bottom-simulating reflectors (BSRs) and high-amplitude reflectors (HARs)

In the Sea of Okhotsk, BSRs are widespread and easily recognized on seismic profiles obtained using a relatively low-frequency

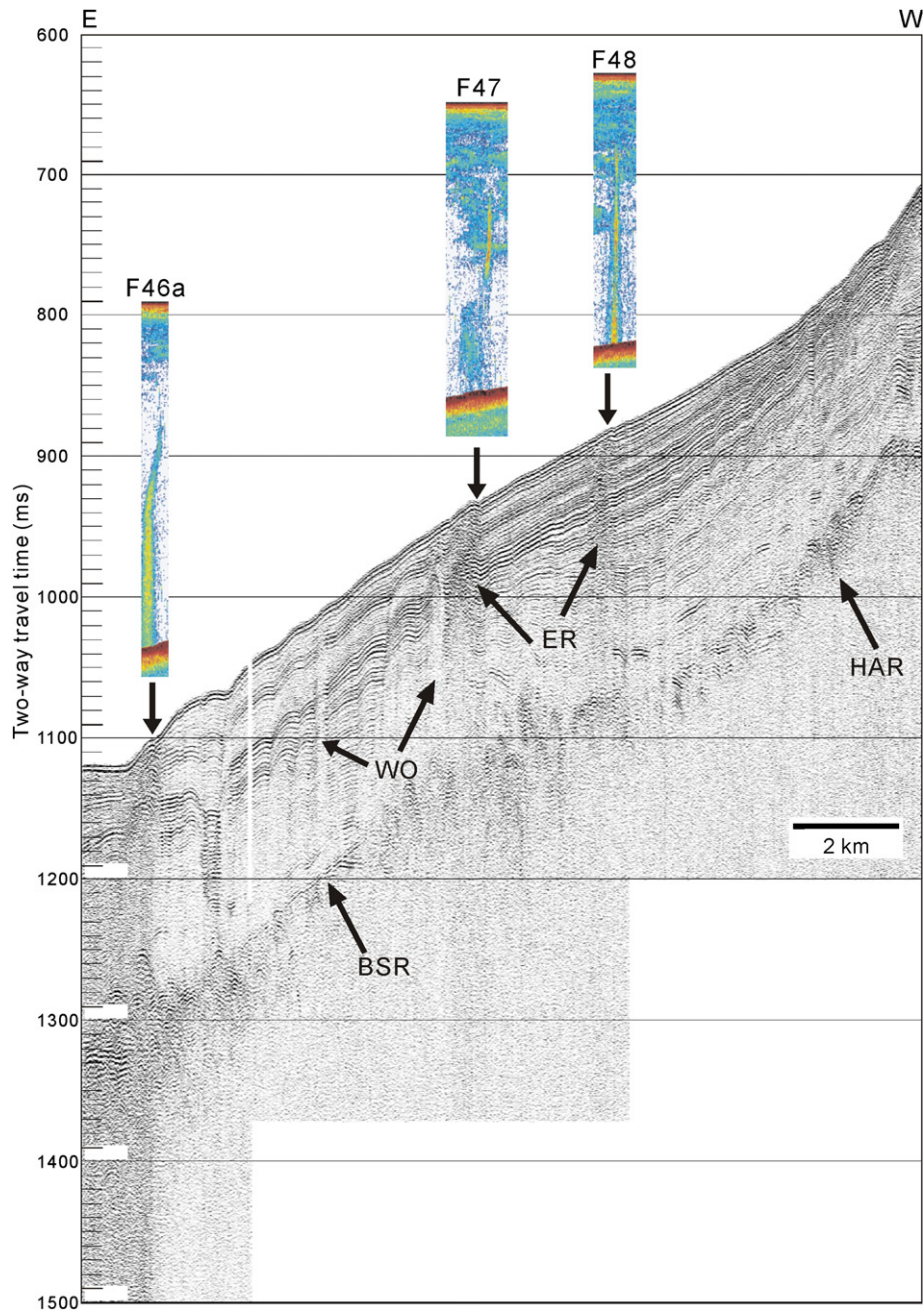


Figure 8. Seismic chimneys, bottom-simulating reflectors (BSRs), and high-amplitude reflectors (HARs) in a sparker seismic profile. The nature of their internal reflection defines two chimney types: wipe-out (WO) and enhanced-reflection (ER) chimneys. Gas flares are detected only at ER chimneys. The BSRs are discontinuous, and HARs are commonly present below the BSR horizon. This seismic line partly overlaps with Fig. 3d. Superimposed gas flare images are from Fig. 3d (not scaled). Loci where F46a, F47, and F48 are emitted correspond to the Kitami, KOPRI, and POI structures. See Fig. 2 for location.

airgun source (Lüdmann and Wong, 2003). BSRs are rare, however, on the high-resolution seismic profiles obtained in the study area. For example, a BSR subparallel to the seafloor appears as a weak straight reflector with short continuity (<4 km) at 180 ms two-way travel-time (TWTT) below the seafloor (Fig. 8). The BSR cuts clearly across stratigraphic reflectors and seems to have reverse polarity to the seafloor reflector. Similar weak BSRs have been reported from high-resolution seismic profiles in other studies (Vanneste et al., 2001; Wood et al., 2002; Cooper and Hart, 2002).

In contrast to BSRs, chaotic high-amplitude reflections (HARs) are widespread at 150–200 ms TWTT below the seafloor and generally mimic the seafloor topography. The BSR reflector is above the HARs. It is inferred that the tops of the HARs generally

correspond to the BSR depth (i.e., the base of the GHSZ). The HARs are thought to be caused by strong acoustic impedance contrasts due to free gas accumulation below the BSR (Vanneste et al., 2001). Free gas would be trapped beneath hydrate-bearing sediment due to the reduced effective porosity and permeability above (Ecker et al., 1998). Transparent or weak reflections in the lower section of the sediment above the BSR or HARs may be attributed to amplitude blanking by a high concentration of gas hydrates near the base of the GHSZ (Lee and Dillon, 2001).

4.4.3. Gas chimneys

High-resolution seismic profiles show gas chimneys as near-vertical acoustic structures in the sediment. Chimneys initiate

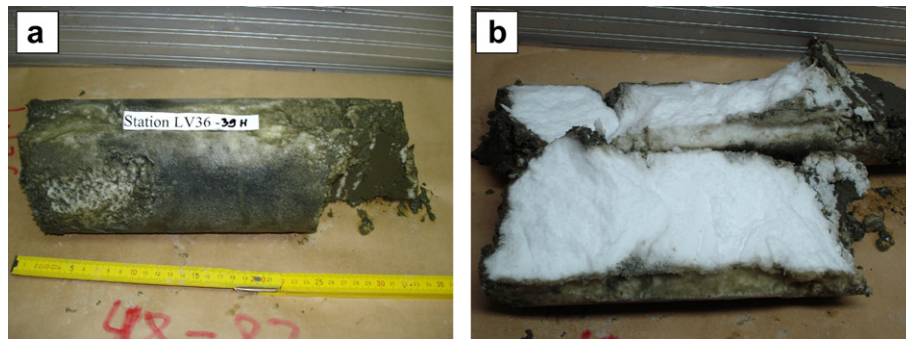


Figure 9. (a) A pure gas-hydrate chunk (35-cm long and 13-cm in diameter) retrieved at the KOPRI structure and (b) its two halves. It was recovered at the sub-bottom depths of 48–53 cm using 5.5-m long gravity corer. See Figs. 2 and 8 (F47) for sampling location.

below the gas hydrate stability zone, and some of them reach the seafloor (Fig. 8). The chimneys that appear on seismic profiles form two groups based on seismic characteristics: (1) narrow (about 100–200 m wide), confined, white-colored wipeout (little or no coherently reflected seismic energy) chimneys (WO in Fig. 8), and (2) wide (>500 m), diffuse, dark-colored (enhanced reflection) chimneys (ER in Fig. 8). Not all wipeout chimneys reach the seafloor, but most of the enhanced reflection chimneys do. Locations where the enhanced reflection chimneys reach the seafloor correspond to mounds on the seafloor (Fig. 8).

4.5. Ground-truthing

4.5.1. Gas hydrates

Nineteen new gas hydrate accumulations were discovered at gas flare sites in the vicinity of gas seeps (yellow stars in Fig. 2b). Gas hydrates were retrieved using a 5.5-m long gravity corer and occurred with various structures in the sediments; lenticular-bedded, micro-aggregates, vein and void-filling, and massive hydrates (Mazurenko et al., 2009). Figure 9 shows a remarkable gas hydrate sample collected at flare site F47 (KOPRI structure) at a water depth of 680 m (see Figs. 2 and 8 for location). The sample is a 35-cm-long chunk of pure methane hydrate. The methane

content of the sample is almost 100%, and the origin of methane is microbial ($\delta^{13}\text{C} = -67\text{‰}$; Hachikubo et al., 2009; Shoji et al., 2009).

4.5.2. High methane concentrations in the water column

Gas analyses of seawater at several water depths were conducted at gas flare sites F46a–48. Anomalously high methane concentrations were measured near the seafloor at these sites (Fig. 10). The concentration was approximately 5000 nl/l at F47, a value that is 100 times that of the background concentration (50 nl/l; Millero, 1996). The lowest value was at F48, but was nonetheless three times the background value. The origin of the methane gas was also microbial (Hachikubo et al., 2009).

5. Discussion

5.1. Seep distribution

In the study area on the NESS, 157 seeps are clustered to form eleven distinct fields (S1–S11) in three zones (northern, central, and southern) (Fig. 11a). Only four seep-related structures are located outside the identified fields.

The northern zone contains only one field, S1, which is just south of a canyon (CA in Fig. 11b). S1 is on the lower slope between 735 and 900 m depth and consists of seven seeps that form a weakly east-trending array. The seep density of the field is one per 1 km^2 .

In the central area (between $54^{\circ}20'\text{N}$ and $54^{\circ}35'\text{N}$), six densely spaced fields (S2–S7) form a weakly east-northeast-trending array. Field S1 is at least 15 km away from this zone, and seafloor seeps are absent on the slope between S1 and this zone (Figs. 2 and 11a), suggesting geological discontinuity between the two zones. Field S2 includes nine seeps at 560–715 m depth. Five of the seeps are near a narrow, northwest-trending bench on the slope. Seep density in the field is $1/\text{km}^2$. Roughly north-trending S3 is the most dense seep field, located at depths of 665–885 m. Thirty-two seeps are present in this field, and seep density is $3/\text{km}^2$. Density contour lines in the field are stretched in two directions: NE–SW and NW–SE. Several of the large, active seeps shown in Fig. 8 form a west-trending line at $54^{\circ}30'\text{N}$. Field S4 consists of 13 seeps at depths of 915–1060 m and has an isometric outline. Seep density is $2/\text{km}^2$. Field S5 includes 6 seeps on the lower slope at depths of 1055–1095 m. Four of these are densely spaced along a west-trending zone. Seep density is $1/\text{km}^2$. Field S6 includes six seeps at depths of 450–700 m and forms a compact west-trending group. Seep density is $1/\text{km}^2$. Field S7 contains 15 seep structures at depths of 770–965 m. The field is weakly west-trending, and seep density is $2/\text{km}^2$.

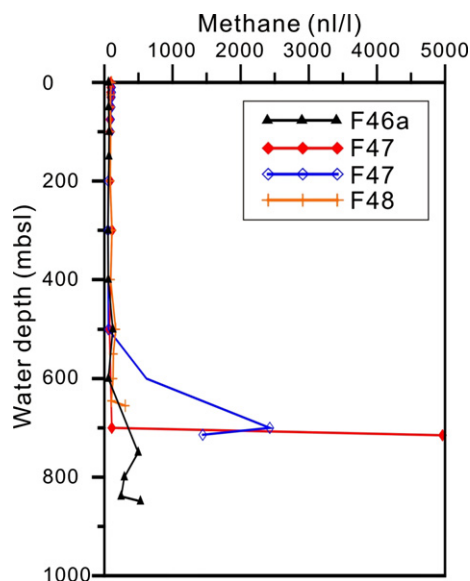


Figure 10. Methane concentration at flare sites (F46–48) shown in Figs. 3d and 8. It is noted that high concentration in methane occurs near the seafloor.

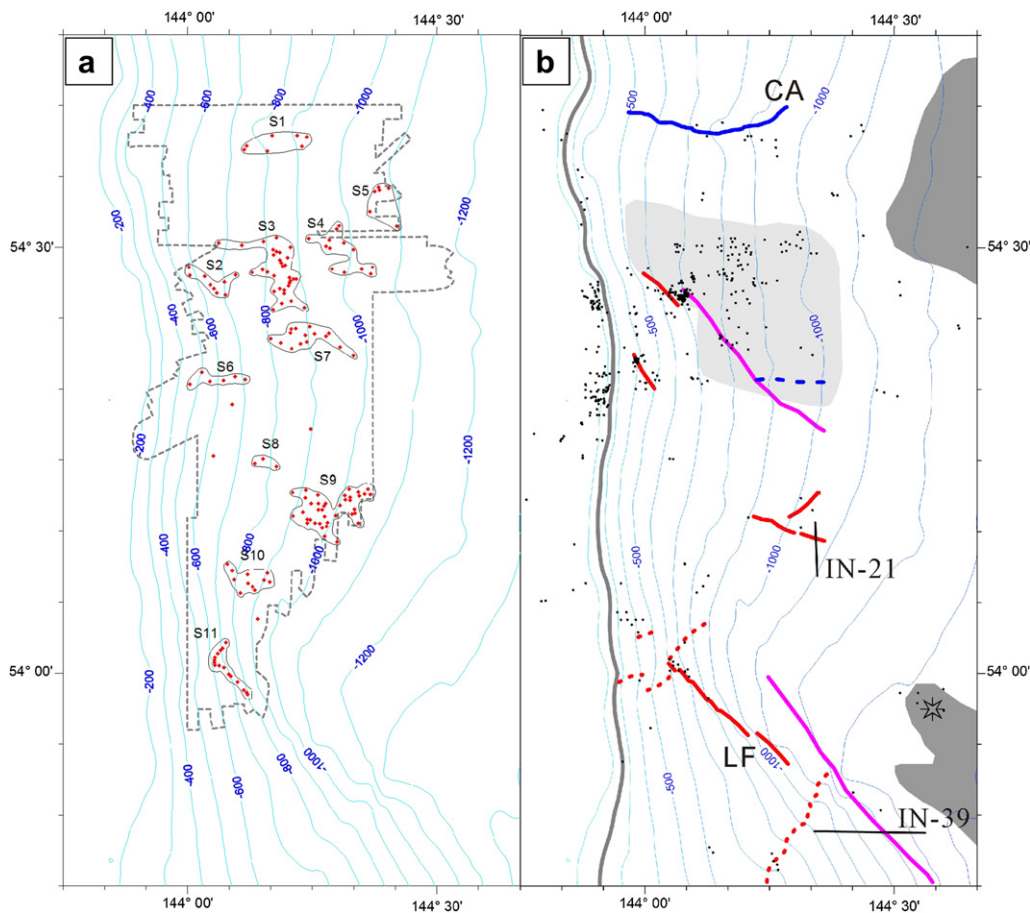


Figure 11. Geological features and distribution of gas flares and side-scan sonar (SSS) structures. (a) Distribution of SSS structures (red diamonds). Seep fields S1 to S11 are within the SSS mapping area (dashed line). (b) Interpreted tectonic map with gas flare locations (black dots). Thick gray line indicates shelf break at 200-m water depth. Red lines mark faults associated with seafloor topography. Magenta lines mark inferred faults covered by sediment. Dashed red lines indicate canyons or slide scars that may be faults. Star indicates possible mud volcano. Solid blue line shows canyon axis; dashed blue line marks inferred canyon axis. Pale and dark gray areas indicate slide scar and areas of hummocky relief, respectively. Contour interval is 100 m. CA = canyon; LF = Lavrentyev faults. (For interpretation of the references to colour in this figure legend, the reader is referred to the web version of this article.)

The southern zone has four seep fields (S8-S11) that form a northeast-trending array (Fig. 11a). The area southeast of this array was not covered by the SSS survey, but several gas flares were identified by hydroacoustic surveying during other expeditions (Figs. 2b and 11b). Three seeps are present in the area between the central and southern zones, another area that lacks extensive seep activities. Field S8 is small and west-trending and contains three seeps at depths of 625–825 m; seep density is 1/km². The largest seep field in the study area is S9, consisting of 39 seeps. This field is on the lower slope at depths of 860–1050 m. Seep density is

approximately 3/km². Seeps in S9 form two diffuse arrays that trend northwest and northeast. The eleven seeps of S10 are on the mid-slope at depths of 750–950 m, and seep density is 2/km². Field S11 includes 16 seeps at depths of 625–800 m. These seeps are aligned to form northwest- and northeast-trending chains. The chains coincide with the trace of the Lavrentyev Fault (LF; Fig. 11b) and its conjugate. Seep density is 2/km².

In summary, the fields contain from 3 up to 39 seepage structures and locate in depth interval 450–1095 m; the density of the seepage structures changes from 1 to 3 per km² (Table 1). They align

Table 1
Characteristics of the seep fields. CH = CHAOS, HI = Hieroglyph, KI = Kitami, KO = KOPRI, KT = KIT, SO = Soloviev, PO = POI structures. See Fig. 2 for location.

Zone	Field number	Water Depth interval (m)	Amount of seeps	Density per km ²	Tectonic position	Gas hydrate sites
Northern	S1	735–900	7	1	Canyon southern side	SO
Central	S2	560–715	9	1	Submarine slide	–
	S3	665–885	32	3	Submarine slide	HI, KI, KO, PO
	S4	915–1060	13	2	Submarine slide	CH
	S5	1055–1095	6	1	Unknown	–
	S6	450–700	6	1	Submarine slide	GI
	S7	770–965	15	2	Submarine slide	–
	Southern	S8	625–825	3	1	Unknown
S9		860–1050	39	3	NE/NW faults	–
S10		750–950	11	2	?	–
S11		625–800	16	2	Lavrentyev Fault	KT

in WE (S1, S6, S7), NE and NW (S2, S10, S11) direction, or have irregular shapes (S3–S5, S9).

5.2. Controls on seep distribution

The area covered by the SSS survey is bounded by a canyon to the north and the LF to the south (Fig. 2). This area corresponds to part of the slope that was exposed by submarine mass wasting (Wong et al., 2003). Figure 11b shows a structural map of the study area with the locations of seeps as determined from hydroacoustic and sonar investigations. The map shows a distinct correlation in the majority of cases between seep distribution and the shelf break, faults, canyon, and submarine slide.

The slope-parallel distribution of gas flares near the shelf break may be related to gas hydrate dissociation above the upper boundary of the GHSZ at ~300 m water depth. Echograms obtained near the shelf break show a diffuse gas emission pattern that is different from the focused appearance of flares on the slope (Fig. 12).

The northwest-trending LF is a major fault with a topographic offset of more than 100 m. The fault extends from below 1250 m water depth to the shelf break (Fig. 11b; Dullo et al., 2004; Mazurenko et al., 2006). Although the fault expresses no topographic differential below 1250-m water depth, it is evident on the seismic profiles (Fig. 13). Another distinct fault is a northeast-trending conjugate fault of the LF (Dullo et al., 2004). Seep field S11 is at the northwestern end of the LF. Nine of its 16 seeps are linearly aligned along the LF, and the rest are densely arranged along its conjugate.

Many seeps in the central and southern zones are aligned along faults that have two distinct trends (Fig. 11). The longest fault trends northwest across the central zone; it is easily recognized on the seismic profiles, but is not expressed topographically on the seafloor. In contrast, two short northwest-trending faults on the upper slope in the central zone have distinct topographic expressions.

A canyon near the northern border of the study area forms a west-trending feature. The canyon is spatially associated with gas flares and seepage structures of S1 (Fig. 11). The west-trending canyon is up to 2 km wide and 150 m deep and is arc-shaped on the SSS mosaic (Fig. 2). Its northern slope is steeper than its southern slope. The canyon appears to be erosional and vanishes at the toe of the slope. Seeps and gas flares are absent inside the canyon.

Based on a marked difference in slope morphology between the northern and southern slopes of the LF, Wong et al. (2003) suggested that the northern slope had experienced submarine sliding.

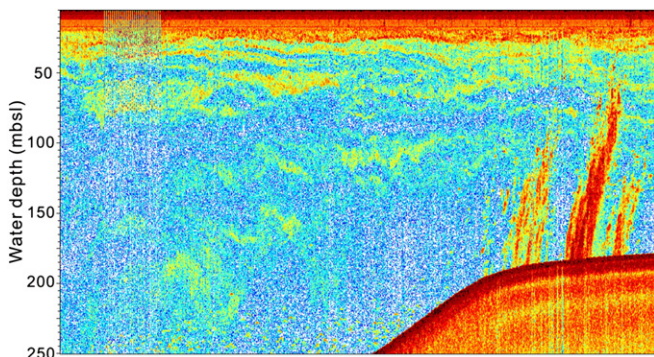


Figure 12. An echogram of gas flares showing diffuse gas emission pattern at the shelf break.

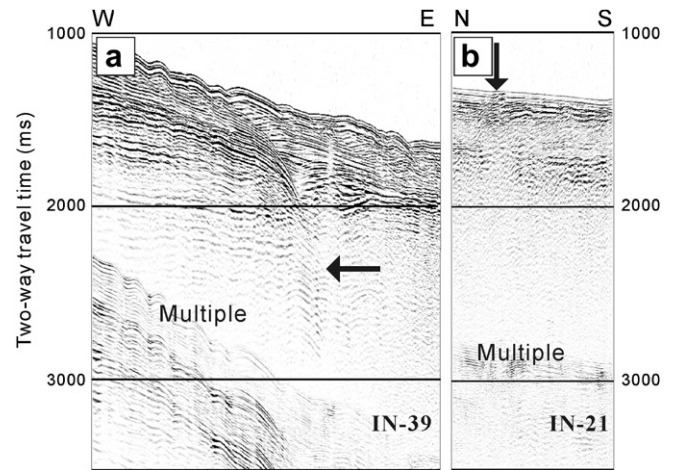


Figure 13. Seismic profiles showing structures of (a) the Lavrentiev Fault and (b) one of the NW-striking faults. Arrows mark faults. See Fig. 11b for location.

Assuming that a 70-km-long section of the slope was involved in the most recent mass-wasting events, they calculated the volume of sediment lost to be about 660 km³. In this study, we suggest a submarine slide area in the central zone (a gray zone in Fig. 11b). Although the slide is relatively weakly expressed and masked by sediment, it has some slide features: slide scars, a pressure zone, and an area containing large clasts of sedimentary material (Baranov et al., 2008). Most of the seeps in the central zone are confined to this submarine slide zone. Seeps are concentrated along a northwest-trending slide scar and along shallow reverse faults that are confined to a north- and east-trending pressure zone.

5.3. ER gas chimneys: active pathways for gas migration to the seafloor

High-resolution seismic and hydroacoustic profiles obtained simultaneously during several expeditions show remarkable correlation between the subsurface ER chimneys and gas flares in the water column. For example, flares F46a, F47, and F48 were associated with topographic mounds where the ER chimneys reach the seafloor (Fig. 8), whereas no gas flares are associated with two WO chimneys that are located between F46a and F47.

On the seismic profile, the ER chimneys show reflection characteristics that are similar to those of HARs (both frequency and amplitude) near the base of the GHSZ. Enhanced reflections of chimneys may be caused by minor gas accumulations migrating laterally into surrounding permeable layers from pathways (mainly faults) in chimneys (Judd and Hovland, 2007). Gas in the permeable layers may cause a significant increase in the impedance contrast of the sediment layers involved, resulting in high-amplitude reflections (Cooper and Hart, 2002; Lüdmann and Wong, 2003). Liu and Flemings (2006) summarized three mechanisms for the co-existence of gas and gas hydrate in the GHSZ: 1) gas flow that is not in equilibrium with its surroundings because of kinetic effects; 2) limited water availability when gas is supplied in excess to its proportion in hydrate; and 3) perturbation of the P–T boundary that defines the GHSZ by advecting warm fluids, capillary effects in fine-grained sediment, or high pore-water salinity. One or several of these conditions could enable gas to exist locally in or near a pathway in the GHSZ. Conditions that would allow gas to exist in or near a pathway in gas-hydrate-bearing sediment are identical to those beneath the base of the GHSZ, which explains why

ER chimneys exhibit seismic reflections that are similar to those of HARs at the depth of the BSR (Fig. 8).

On the profile, enhanced reflections of chimneys are more distinct in the shallower part of the gas-hydrate-bearing sediment than in the deeper part. This could be attributed to little lateral saturation of gas from the pathway into surrounding low-permeability layers owing to a high concentration of gas hydrates in the deeper part, and/or a rapid increase of free gas extracted from gas-bearing fluid that is caused by a decrease of methane solubility toward the seafloor inside the GHSZ (Zatsepin and Buffett, 1997).

Under ER chimneys, a BSR is absent, and HARs are elevated and heavily disturbed. This means that the distribution of gas hydrate stability is severely perturbed by the mechanism that enables free gas to migrate along chimneys, possibly with water as heat carrier.

The ER chimneys are interpreted as pathways for active gas transport (mainly methane) upward to the seafloor through gas hydrate-bearing sediment, whereas WO chimneys represent inactive pathways that may be former ER chimneys that are now choked with gas hydrate.

5.4. Formation of the circular high backscatter patterns of active seeps

As shown in Figures 4–7, the circular seepage structures with high backscatter intensity are very common in the study area. They are generally associated with gas flares, bathymetric mounds, high subsurface reflections, gas chimneys and shallow gas-hydrate deposits. Based on all our observations in this study and earlier published results, we propose a model for the formation of the circular high backscatter patterns of active seeps. Free gas from below the BGHS rises to the seafloor through the sediments along gas migration pathway, which appears as an ER gas chimney below the seeps (Fig. 8). Close to the seafloor the free gas bubbles can form massive gas-hydrate deposits as seen in Figure 9 by pushing apart the sediments. This subsurface hydrate formation is only possible at shallow sediment depth as a certain force is needed to push apart the sediments (Flemings et al., 2003) or/and as bottom seawater can supply sufficient water for hydrate formation. Hydrate formation occurs around the pathway in a concentric pattern, which leads to a sort of “hydrate halo”, a circular feature as described by Soloviev and Ginsburg (1997). Formation and accumulation of pure hydrates in the subsurface may also lead to up-doming of the sediments such that the sites are traceable as mounds of some meters height in the bathymetry (Figs. 6a and 8). Expansion associated with gas hydrate formation was proposed as a mechanism to form the mounds (>10 m high and >100 wide) in the Santa Monica Basin (Paull et al., 2008). The deposition of hydrate close to the seafloor is also likely to explain the high surface reflections in the sediment shown in Figure 7a and b. This is similar to the observation of shallow hydrates at pockmarks at the Congo fan (Sahling et al., 2008). The bubbles that do not form hydrates in the sediments are emitted into the water column where they are recorded as flares by echosounder or high-reflectivity gas emission in side-scan sonar.

6. Conclusions

The northeastern Sakhalin continental slope (NESS) of the Sea of Okhotsk is characterized by an abundance of gas seeps and gas hydrates. Multidisciplinary surveys have been carried out to investigate gas seepage and gas hydrate accumulation and led to the following conclusions:

1. In water depths of 300–1000 m on the NESS (between 53°45'N and 54°45'N), 161 gas seeps were detected in a 2000-km² area during expeditions undertaken from 2003 to 2007. The gas seeps are widespread within the gas hydrate stability zone.
2. Ongoing gas seepage was indicated by various phenomena: strong hydroacoustic anomalies (gas flares), side-scan sonar structures with high backscatter intensity (seepage structures), bathymetric features (pockmarks and mounds), gas- and gas-hydrate-related seismic features (bottom-simulating reflectors, gas chimneys, high-amplitude reflectors, and acoustic blanking), high methane concentrations in seawater, and near-bottom gas hydrate occurrence.
3. Indicators of gas seepage are commonly clustered at active seeps. For example, a gas flare is spatially associated with a topographic mound with strong backscatter intensity, below which acoustic blanking and a gas chimney are present.
4. The spatial distribution of gas seeps in the study area is controlled by four structural elements: faults, the shelf break, submarine valleys and submarine slides. Northwest- and northeast-trending fault systems, including the Lavrentyev Fault, are the most important control on seep distribution.
5. Gas chimneys showing enhanced reflection (ER) on high-resolution seismic profiles are interpreted as active pathways in which gas (mainly methane) is migrating upward to the seafloor. In addition to active gas flares, ER chimneys are a good indicator of active seepage.

Acknowledgments

We thank the captain and crew of the R/V Akademik M. A. Lavrentyev and all participants of the CHAOS (Carbon Hydrate Accumulations in the Okhotsk Sea) and SSGH (Sakhalin Slope Gas Hydrates) projects. We are grateful to anonymous reviewers and the editor for the constructive comments that improved the manuscript considerably. This study has been supported by Korean Ministry of Land, Transport and Maritime Affairs R&D grants PM10030, PM10040 and Japan Society for the Promotion of Science KAKENHI 18206099 and Presidium of Russian Academy of Sciences, Programme No. 20.

References

- Astakhov, A., Botsul, A., Biebow, N., Derkachev, A., Fessler, S., Gobarenko, S., Kaiser, A., Nikolayeva, R., Tiedemann, R., Werner, R., 2000. Paleocyanography and sedimentology. In: Biebow, N., Ludmann, T., Karp, B.Y., Kulinich, R. (Eds.), KOMEX: Kurile-Sea of Okhotsk Marine Experiment. Cruise Reports: KOMEX V and KOMEX VI, R/V 'Professor Gagarinsky' Cruise 26 and M/V 'Marshal Gelovany' Cruise I. GEOMAR, Kiel, pp. 189–209. Report 88.
- Baranov, B.V., Jin, Y.K., Shoji, H., Obzhirrov, A., Dozorova, K.A., Salomartin, A., Gladyshev, V., 2008. Gas Hydrate System of the Eastern Sakhalin Slope: Geophysical Approach. Scientific Report of the Sakhalin Slope Gas Hydrate Project 2007. Korea Polar Research Institute, Incheon, p. 116.
- Biebow, N., Hutten, E., 1999. Cruise Report KOMEX I and II: RV Professor Gagarinsky Cruise 22, RV Akademik M.A. Lavrentyev Cruise 28. Report No. 82. GEOMAR.
- Biebow, N., Kulinich, R., Baranov, B., 2003. KOMEX Cruise Report: RV Akademik M. A. Lavrentyev Cruise 29, Leg I and Leg II. Report No. 190. GEOMAR.
- Cooper, A.K., Hart, P.E., 2002. High-resolution seismic-reflection investigation of the northern Gulf of Mexico gas-hydrate-stability zone. *Marine and Petroleum Geology* 19, 1275–1293.
- Dickens, G.R., Quinby-Hunt, M.S., 1994. Methane hydrate stability in seawater. *Geophysical Research Letters* 21, 2115–2118.
- Dickens, G.R., O'Neil, J.R., Rea, D.K., Owen, R.M., 1995. Dissociation of oceanic methane hydrate as a cause of the carbon isotope excursion at the end of the Paleocene. *Paleoceanography* 10, 965–971.
- Dullo, W.-Chr., Biebow, N., Georgeleit, K., 2004. SO178 KOMEX Cruise Report Kiel, p. 125.
- Ecker, C., Dvorkin, J., Nur, A., 1998. Sediment with gas hydrates: internal structure from seismic AVO. *Geophysics* 39, 759–769.
- Flemings, P.B., Liu, X., Winters, W.J., 2003. Critical pressure and multiphase flow in Blake Ridge gas hydrates. *Geology* 31, 1057–1060.

- Fournier, M., Jolivet, L., Huchson, P., Sergeev, K.F., Osorbin, L.S., 1994. Neocene strike-slip faulting in Sakhalin and Japan Sea. *Journal of Geophysical Research* 99, 2701–2725.
- Gaedicke, Chr., Baranov, B.V., Obzhairov, A.I., Lelikov, E.P., Belykh, I.N., Basov, E.I., 1997. Seismic stratigraphy, BSR distribution and venting of methane rich fluid west off Paramushir and Onekotan Islands, northern Kuril. *Marine Geology* 116, 259–276.
- Ginsburg, G.D., Soloviev, V.A., Cranston, R.E., Lorenson, T.D., Kvenvolden, K.A., 1993. Gas hydrates from the continental slope, offshore Sakhalin Island, Okhotsk Sea. *Geo-Marine Letters* 13, 41–48.
- Gorbarenko, S.A., Kovalyukh, N.N., Odinkova, L.Yu., Rybakov, V.F., Tokarchuk, T.N., Shapovalov, V.V., 1990. Upper Quaternary sediments of the Sea of Okhotsk and the reconstruction of paleoceanologic conditions. *Geology of Pacific Ocean* 6, 309–330.
- Greinert, J., Artemov, Y., Egorov, V., De Batist, M., McGinnis, D., 2006. 1300-m-high rising bubbles from mud volcanoes at 2080 m in the Black Sea: hydroacoustic characteristics and temporal variability. *Earth and Planetary Science Letters* 244, 1–15.
- Hachikubo, A., Sakagami, H., Minami, H., Nunokawa, Y., Shoji, H., Matveeva, T., Jin, Y.K., Obzhairov, A., 2009. Isotopic composition and crystallographic properties of gas hydrate in the Sea of Okhotsk. *Journal of Geography* 119, 207–221.
- Hachikubo, A., Krylov, A., Sakagami, H., Minami, H., Nunokawa, Y., Shoji, H., Matveeva, T., Jin, Y.K., Obzhairov, A., 2010. Isotopic composition of gas hydrates in subsurface sediments from offshore Sakhalin Island, Sea of Okhotsk. *Geo-Marine Letters* 30, 313–319.
- Heeschen, K., Tréhu, A., Collier, R.W., Suess, E., Rehder, G., 2003. Distribution and height of methane bubble plumes on the Cascadia Margin characterized by acoustic imaging. *Geophysical Research Letters* 30, 1643. doi:10.1029/2003GL016974.
- Hovland, M., Judd, A.G., 1988. Seabed Pockmarks and Seepages: Impact on Geology, Biology and the Marine Environment. Graham and Trotman Ltd., London, p. 293.
- Judd, A.G., 2003. The global importance and context of methane escape from the seabed. *Geo-Marine Letters* 23, 147–154.
- Judd, A., Hovland, M., 2007. Seabed Fluid Flow. Impact on Geology, Biology, and the Marine Environment. Cambridge University Press, Cambridge, UK, p. 475.
- Katz, M.E., Pak, D.K., Dickens, G.R., Miller, K.G., 1999. The source and fate of massive carbon input during the latest Paleocene thermal maximum. *Science* 286, 1531–1533.
- Kennett, J.P., Cannariato, K.G., Hendy, I.L., Behl, R.J., 2000. Carbon isotopic evidence for methane hydrate instability during Quaternary interstadials. *Science* 288, 128–133.
- Kharakhinov, V.V., 1998. Tectonics of the Okhotsk Sea Oil and Gas Potential Province. SakhalinNIPImorneft, Okha, p. 77 (in Russian).
- Kvenvolden, K.A., 1993. Gas hydrates-geological perspective and global change. *Review of Geophysics* 31, 173–187.
- Lee, M.W., Dillon, W.P., 2001. Amplitude blanking related to the pore-filling of gas hydrate in sediments. *Marine Geophysical Research* 22, 101–109.
- Liu, X., Flemings, P.B., 2006. Passing gas through the hydrate stability zone at southern Hydrate Ridge, offshore Oregon. *Earth and Planetary Science Letters* 241, 211–226.
- Lüdmann, T., Wong, H.K., 2003. Characteristics of gas hydrate occurrences associated with mud diapirism and gas escaping structures in the northwestern Sea of Okhotsk. *Marine Geology* 201, 269–286.
- MacDonald, I.R., Sassen, I.L.R., Stine, P., Mitchell, R., Guinasso, N.J., 2002. Transfer of hydrocarbons from natural seeps to the water column and atmosphere. *Geofluid* 2, 95–107.
- Matveeva, T., Soloviev, V., Wallman, K., Obzhairov, A., Biebow, N., Poort, J., Salomatin, A., Shoji, H., 2003. Geochemistry of gas hydrate accumulation offshore NE Sakhalin Island (the Sea of Okhotsk): results for the KOMEX-2002 cruise. *Geo-Marine Letters* 23, 278–288.
- Matveeva, T., Soloviev, V., Shoji, H., Obzhairov, 2005. Hydro-Carbon Hydrate Accumulations in the Okhotsk Sea (CHAOS Project Leg I and Leg II). Report of R/V Akademik M.A. Lavrentyev Cruise 31 and 32. Russia Research Institute for Geology and Mineral Resources of the Ocean, VNIIOkeangeologia, St.Petersburg, p. 164.
- Mazurenko, L.L., Obzhairov, A., Shoji, H., Jin, Y.K., Nikoaeva, N., 2006. Hydro-Carbon Hydrate Accumulations in the Okhotsk Sea (CHAOS-II Project). Report of R/V Akademik M.A. Lavrentyev Cruise 36, Vladivostok-St.Petersburg, 2006. p. 127.
- Mazurenko, L.L., Matveeva, T.V., Prasolov, E.M., Shoji, H., Obzhairov, A.I., Jin, Y.K., Poort, J., Logvina, E.A., Minami, H., Sakagami, H., Hachikubo, A., Salomatin, A.S., Salyuk, A.M., Prilepskiy, E.B., Chaos 2003 Scientific Team, 2009. Gas Hydrate Forming Fluids on the NE Sakhalin Slope, Sea of Okhotsk. In: Long, D., Lovell, M.A., Rees, J.G., Rochelle, C.A. (Eds.), *Sediment-hosted Gas Hydrates: New Insights on Natural and Synthetic Systems*. Geological Society of London, Special Publication, vol. 319, pp. 51–72.
- Millero, F.J., 1996. *Chemical Oceanography*, second ed. CRC Press, Inc., Florida, p. 469.
- Naudts, L., Greinert, J., Poort, J., Belza, J., Vangamlelaere, E., Boone, D., Linke, P., Henriot, P., De Batist, M., 2010. Active venting sites on the gas-hydrate-bearing Hikurangi Margin, off New Zealand: diffusive- Versus bubble-released methane. *Marine Geology* 272, 233–250.
- Obzhairov, A.I., 1992. Gas-geochemical manifestations of gas-hydrates in the Sea of Okhotsk. *Alaska Geology* 21, 1–7.
- Paull, C.K., Normark, W.R., Ussler III, W., Cares, D.W., Keaten, R., 2008. Association among active seafloor deformation, mound formation, and gas hydrate growth and accumulation within the seafloor of the Santa Monica Basin, offshore California. *Marine Geology* 250, 258–275.
- Paull, C.K., Ussler III, W., Dillon, W.P., 1991. Is the extent of glaciations limited by marine gas-hydrates? *Geophysical Research Letters* 18, 432–434.
- Rozhdestvenskiy, V.S., 1986. Evolution of the Sakhalin folds system. *Tectonophysics* 127, 331–339.
- Salomatin, A., Lee, B., Obzhairov, A., 2008. Hydroacoustic investigations. In: Shoji, H., Jin, Y.K., Obzhairov, A. (Eds.), *Operation Report of Sakhalin Slope Gas Hydrate Project 2007*, R/V Akademik M.A. Lavrentyev Cruise 43, pp. 21–24.
- Sauter, E.J., Muyakshin, S.I., Charlou, J.-L., Schluter, M., Boetius, A., Jerosch, K., Damm, E., Foucher, J.-P., Klages, M., 2006. Methane discharge from a deep-sea submarine mud volcano into the upper water column by gas hydrate-coated methane bubbles. *Earth and Planetary Science Letters* 243, 354–365.
- Sergeev, K.Ph., 2004. Tectonics and Hydrocarbon Potential of the Okhotsk Sea. Russian Academy of Sciences FEB, Inst. Mar. Geol. & Geophys., Vladivostok (in Russian).
- Sahling, H., Bohrmann, G., Spiess, V., Bialas, J., Breitzke, M., Ivanov, M., Kasten, S., Krastel, S., Schneider, R., 2008. Pockmarks in the Northern Congo Fan area, SW Africa: complex seafloor features shaped by fluid flow. *Marine Geology* 249, 206–225.
- Shoji, H., Jin, Y.K., Obzhairov, A., Salomatin, A., Baranov, B., Gladyshev, V., Hachikubo, A., Minami, H., Yamashita, S., Takahashi, N., 2009. Methane hydrates and plumes in the Sea of Okhotsk. *Journal of Geography* 119, 175–193.
- Soloviev, V.A., Ginsburg, G.D., 1994. Formation of submarine gas hydrates. *Bulletin of the Geological Society of Denmark* 41, 86–94.
- Soloviev, V.A., Ginsburg, G.D., 1997. Water segregation in the course of gas hydrate formation and accumulation in submarine gas-seepage fields. *Marine Geology* 137, 59–68.
- Soloviev, V.A., Ginsburg, G.D., Douglas, V.K., Cranston, R., Lorenson, T., Alekseev, I.A., Baranova, N.S., Ivanova, G.A., Kazazaev, V.P., Lobkov, V.A., Mashirov, Y.G., Natorkhin, M.I., Obzhairov, A.I., Titaev, B.F., 1994. Gas hydrates of the Okhotsk Sea. *Otechestvennaya Geologiya* 2, 10–16 (in Russian).
- Tikhonov, I.N., Kim, C.U., 2010. Confirmed prediction of the 2 August 2007 MW 6.2 Nevsk earthquake (Sakhalin Island, Russia). *Tectonophysics* 485, 85–93.
- Vanneste, M., De Batist, M., Golmshtok, A., Kremlev, A., Versteeg, W., 2001. Multi-frequency seismic study of gas hydrate-bearing sediments in Lake Baikal, Siberia. *Marine Geology* 172, 1–21.
- Wong, H.K., Lüdmann, T., Baranov, B.V., Karp, B.Y., Konerding, P., 2003. Bottom current-controlled sedimentation and mass wasting in the north-western Sea of Okhotsk. *Marine Geology* 201, 287–305.
- Wood, W.T., Gettrust, J.F., Chapman, N.R., Spence, G.D., Hyndman, R.D., 2002. Decreased stability of methane hydrates in marine sediments owing to phase-boundary roughness. *Nature* 420, 656–660.
- Worrall, D.M., Kruglyak, V., Kunst, F., Kuznetsov, V., 1996. Tertiary tectonics of the Sea of Okhotsk, Russia: far-field effects of the India-Eurasia collision. *Tectonics* 15, 813–826.
- Zatsepina, O.Y., Buffett, B.A., 1997. Phase equilibrium of gas hydrate: implications for the formation of hydrate in the deep sea floor. *Geophysical Research Letters* 24, 1567–1570.
- Zonenshayn, L.P., Murdmaa, I.O., Baranov, V., Kuznetsov, A.P., Kuzin, V.S., Ku'zmin, M.I., Avdeyko, G.P., Stunzhasm, P.A., Lukashin, V.N., Barash, M.S., Valyashko, G.M., Demina, L.L., 1987. An underwater gas source in the Sea of Okhotsk. *Oceanology* 27, 598–602.